

**BIOMECHANICAL CHARACTERIZATION OF THE STENTED ARTERY.**  
**COMPUTATIONAL SOLID MECHANICAL ASPECTS**

**Gerhard A. HOLZAPFEL<sup>1,2</sup>, Dimitrios E. KIOUSIS<sup>1</sup>**

*<sup>1</sup>Institute for Biomechanics, Centre for Biomedical Engineering  
Graz University of Technology, Austria*

*<sup>2</sup>Department of Solid Mechanics, School of Engineering Sciences  
Royal Institute of Technology, Stockholm, Sweden*

**Published in**

G.A. Holzapfel and D.E. Kiousis: Biomechanical characterization of the stented artery. Computational solid mechanical aspects. In: N. Chakfé, B. Durand and J.-G. Kretz (eds.), "ESVB 2007 – New Technologies in Vascular Biomaterials. Fundamentals About Stents II", Chapter 2, Europrot, Strasbourg, France (2007), 11-23.

## **ABSTRACT**

*Since stent design and the stent deployment technique are one cause for the success or failure of angioplasty treatments. Biomechanics has an important role in characterizing the solid and fluid mechanical environment that is achieved due to stent implantation. Supra-physiological loading conditions may lead to stress-induced wall damage, local interaction of the stent struts with the artery wall to focal vascular trauma, and the disturbed flow to non-physiological wall stresses. The mechanical changes that occur during and after dilation of the artery activate mechanobiological processes and may finally lead to in-stent restenosis characterized by a fibroproliferative response and by increased matrix production.*

*There are only a very few approaches documented in the literature that address the solid mechanical aspects of stenting. The present work summarizes one efficient methodology able to predict the changes in the mechanical environment of stenotic arteries that occur during the interaction with stents, while fluid dynamical aspects that may also drive clinical failures are not addressed here. The methodology is based on a computational strategy which allows a deeper insight in the development of mechanical strains and contact pressures during and after artery dilation.*

*In particular, the stent interaction with a patient-specific, atherosclerotic lesion of a femoral artery is modeled, and two different strut thicknesses of the stent are analyzed. The respective lumen gain and the pressure between the stent struts and the surface of the intima are visualized, and consequences discussed.*

## **INTRODUCTION**

Balloon angioplasty with stent placement is a well established and effective vascular reconstructive procedure aiming to reduce the severity of atherosclerotic stenosis. Its popularity arises due to its less invasive nature (compared to surgical alternatives) and its better clinical outcome (compared to balloon angioplasty without stenting<sup>1,2</sup>). Just in the US a total of 574.000 angioplasty procedures with stenting were performed in 2003<sup>3</sup>. In the US the stent market has now expanded to \$5 billion per year.

Despite the constantly increasing success rate of stenting through technological progresses in the stent design and drug coatings on the stents' surface<sup>4</sup>, the procedure can still fail because of restenosis in stents, which occurs in 30-60% of patients with complex lesions<sup>5</sup>. In coronary arteries when treated with bare-metal stent designs the restenosis rates range from 20%–40%<sup>6</sup>. Although, drug-eluting stents (DESs) have limited restenosis in coronary arteries, the restenosis rate for drug-eluting or bare-metal stents deployed in the periphery is still unsatisfactorily high. In addition, it is worth noting that recently some hospitals (in particular in Sweden) have also reduced the application of DESs to coronary arteries because of the clinical evidence that DESs lead to a higher risk of thrombus. Hence, the biomechanical and biochemical characterization of arteries stented with a DES, a bare-metal stent or a biodegradable (polymer) stent is of significant academic, industrial, and clinical importance since the mechanochemistry of the environment affects the restenosis rate and the clinical outcome of stenting.

Angioplasty with stenting represents a mechanical solution for a clinical problem. It is, therefore, comprehensible that its success or failure depends not only on the stenosis type but also on the design parameters defining the stent's mechanics such as the related material and

the geometry of the stent cells and struts and the deployment technique. In this respect see also the clinical ISAR-STEREO studies<sup>6,7</sup>, which identified the stents' geometric characteristics as one of the major elements for defining the biomechanical environment of the stented artery and for reducing or increasing the risk of stress-induced growth such as neointimal hyperplasia that occurs through a complex cascade of events, and that can take months to develop<sup>8</sup>.

Hence, the bottom line in stent treatment is to find a trade-off between maximizing the lumen gain and minimizing the changes in flow patterns (keeping the level of wall shear stresses) and the focal vascular trauma imposed by the struts of the stent. The foreign material in the injured artery may trigger molecular mechanisms, and hence lead to inflammation, granulation and extracellular matrix production<sup>9,10</sup>, which result in re-narrowing of the vessel wall.

Consequently, in the last very few years a significant amount of research effort by bioengineers and mathematicians has been devoted to the development of efficient computational tools to better characterize the changes in the mechanical environment of stenotic arteries that occur during the interaction with stents<sup>11-14</sup>, and to assist clinicians and the stent manufacturing industry. Common target is a refined understanding of the mechanical factors involved in the underlying mechanobiological process, the identification of the post-angioplasty mechanical environment of the artery wall, the optimization of the interventional protocols and finally the improvement of the clinical outcome which might result in new strategies to prevent or reduce restenosis.

A literature study of the aforementioned research effort reveals that the majority of the recently developed computational stent models is based on several assumptions which, to some extent, restrict the biomechanical interpretation of the obtained simulation results. A

relatively large number of works investigates the mechanics of the artery wall, the stent and the balloon catheter separately, while very few studies treat their interaction as a three-dimensional (3D) computational problem<sup>15</sup>. In several publications<sup>13,16</sup>, simplified, axisymmetric geometries are considered for the geometrically complex plaque and artery wall, while the balloon catheter is neglected. Although such simplified approaches have undoubtedly contributed to the current level of understanding of angioplasty mechanics, there is a pressing need to model the actual 3D morphology and the related mechanics in a (patient-specific) realistic way, within a robust 3D computational environment.

The main target of the present text is to outline a computational model able to simulate a patient-based balloon angioplasty procedure including stenting, and to interpret the results appropriately. The focus here is the analysis from a solid mechanics point of view (the artery wall and not the blood flow) according to a recent work<sup>17</sup>.

For fluid dynamical aspects and the related hemodynamics that affect clinical failures of stents the reader is referred to the recent articles by Moore and co-workers<sup>18,19</sup>. The documented methodology uses 3D geometries and experimental data of a stenotic femoral artery with a lesion of type V according to Stary<sup>20</sup>. We model the 3D contact interaction between the involved medical devices (balloon, stent) and the artery wall, and we apply a sophisticated material model in order to describe the typical anisotropic and nonlinear material behavior of a balloon catheter. Finally, the described example aims to predict the outcome of the treatment and to allow deeper insight in the development of mechanical strains and contact pressures during and after artery dilation. In addition, the presented approach has the potential to provide a scientific basis for optimizing treatment procedures and stent geometries and materials, to help stent designers examine new stent designs on a

computational basis, and to assist clinicians in choosing the most suitable stent for a specific stenosis.

## **MODELING ASPECTS**

### *Models for the vessel geometry and the material*

We model the 3D morphology and the tissue response of an atherosclerotic human femoral artery. The considered region of the atherosclerotic lesion is of type V according to the histological classification of Stary<sup>20</sup>. A type V lesion (fibroatheroma) contains mainly reparative smooth muscle cells and fibrous tissue and, additionally, lipid pools of unequal size separated from each other by cells and fibrous tissue. The incorporation of a morphological (patient-specific) 3D model into the computational simulation is one of the strong aspects of the documented approach, since 3D models serve as a basis for purposeful computation, able to characterize the mechanical environment of the complete lesion.

We generate the 3D artery model by means of high-resolution magnetic resonance (MR) images and NURBS surface parameterizations. A detailed description of the imaging acquisition method is documented in the study by Auer et al<sup>21</sup>. For the particular example in question, 41 MR sections of the femoral artery with a distance of 0.8 mm are used. For each scanned section, the outer and inner borders of the artery are automatically traced by a set of points. These points are then fitted by NURBS curves, and finally the curves generated for each section are combined along the artery axis so that the 3D surface of the femoral artery is constructed. The geometric model so obtained is shown in Figure 1.

Healthy artery walls consist of three layers with distinct mechanical properties<sup>22</sup>. Atherosclerotic arteries, however, consist of a heterogeneous composition of tissue components with very different mechanical properties<sup>23-28</sup>, which adds an extra degree of

complexity from the modeling point of view. In a first attempt, however, the artery is modeled as a homogeneous material.

Artery walls are anisotropic materials due to the organized arrangement of the load carrying (collagen fibrils) components<sup>29</sup>. However, in practice, there are several isotropic strain-energy functions used to characterize the mechanical response of artery walls. The one chosen for this example is a rubber-like potential, similar to the one documented in Delfino et al.<sup>30</sup> This model is able to describe the typical stiffening effect of arteries within the high pressure domain. The isochoric part of the strain-energy function is

$$\bar{\Psi} = \mu(\bar{I}_1 - 3) + \frac{k_1}{2k_2} \left\{ \exp[k_2(\bar{I}_1 - 3)^2] - 1 \right\},$$

where  $\bar{I}_1$  is the first invariant,  $\mu$  and  $k_1$  are material parameters with the dimensions of stress, while  $k_2$  is a dimensionless parameter. The passive, quasi-static stress-stretch response of the artery, and consequently the material parameters discussed above, are typically determined through mechanical tests performed on a computer-controlled, high precision tensile machine as documented in Schulze-Bauer et al<sup>31</sup>. Briefly, uniaxial extension tests are performed on axial and circumferential strips extracted from the three layers of 11 non-diseased, but aged, femoral arteries, which have undergone *in vitro* balloon angioplasty. All tissue samples are stretched far beyond the physiological loading domain up to failure in order to capture the range of deformations induced by the stent. The above constitutive model is then fitted to the (averaged) behavior of all three layers in both artery directions. A least-square fitting algorithm provides the values for the three parameters, i.e.  $\mu = 0.033$  MPa,  $k_1 = 2.14$  MPa,  $k_2 = 277.6$ .

### *Models for the stent geometry and the material*

In the presented analysis, one type of stent design is investigated, which is based on the previously commercially available Palmaz-Schatz<sup>TM</sup> (Johnson & Johnson) balloon-expandable stent. The chosen stent geometry is traced from images. It resembles a tube with rectangular slots in its undeformed configuration (Figure 2).

The 3D geometric model of the stent is generated by means of a parametrization algorithm. The developed technique is able to describe the stent's overall dimensions as well as the geometry of its cells. The design parameters of the stent are: stent length, unexpanded diameter, number of cells in the axial and circumferential directions and strut thickness which is considered to have a cylindrical cross section. The advantage of a parametric approach is the automated and fast generation of different stent designs. A systematic parametric study<sup>12,32</sup> could finally lead to optimal, patient-tailored stent designs.

The material of the stent is considered to be stainless steel 316L. For the elastic domain of the material, a neo-Hookean model is used, while its inelastic constitutive response is described through a von Mises-Hill plasticity model with linear isotropic hardening. The Young's modulus is chosen as  $E = 200$  GPa and the Poisson ratio is  $\nu = 0.3$ . The parameters  $\sigma_y = 300$  MPa and  $H_{iso} = 2$  GPa are selected for the yield stress and the hardening modulus, respectively.

### *Models for the balloon geometry and the material*

We consider a Grüntzig-type balloon catheter<sup>33</sup>. This specific catheter is widely used in clinical practice and therefore selected. Although the initial forms of balloon catheters are S- or Z-shaped, the reference configuration of the balloon is in this case modeled as a cylindrical

tube with an external diameter  $D_e = 0.3$  mm, wall thickness  $H = 0.2$  mm, and length  $L = 12$  mm. The dilation of the catheter is characterized by a complex kinematics, where the unfolding process of the balloon is followed by a typically nonlinear, stiffening behavior at a higher pressure level.

In the current approach, the complex unfolding process of the balloon is omitted, while a cylindrically orthotropic model is developed in order to describe the overall mechanical behavior of the balloon. This material model is thoroughly described in Kiouisis et al.<sup>17</sup> and is based on a fiber-reinforced material. Briefly, two material axes are introduced, which are oriented in circumferential and longitudinal directions. The matrix material of the balloon catheter is considered as a (soft) isotropic material. The balloon in the circumferential direction is very soft at its initial configuration but particularly stiff after a predefined stretch limit, while in the longitudinal direction it is assumed to be already stiff at its reference configuration. This phenomenological approach is able to satisfyingly model the mechanical behavior of balloon catheters. The finite element mesh of the balloon in the undeformed and deformed configuration at 8 bar of internal pressure, based on the model described above, is depicted in Figure 3a. The relation between the internal balloon pressure and the external balloon diameter is illustrated in Figure 3b. Note that initially, the balloon expands fast and only a low internal pressure is needed for its deformation. As the pressure exceeds approximately 1 bar, the balloon stiffens significantly and deforms only slightly.

## **COMPUTER SIMULATION**

### *Contact interactions*

In the computational modeling of the contact interaction between the balloon, the stent and the artery wall, three surfaces may interact and need to be specified as contact pairs. The involved pairs are: (i) stent-balloon, (ii) stent-artery and (iii) artery-balloon. In all three cases, the first body is considered as the contractor body and the second as the target. To this end, on the basis of a smooth surface description a sophisticated 3D contact algorithm is used<sup>17</sup> in order to avoid numerical instabilities, which occur when standard facet-based approaches are applied. The simulation is carried out without friction since it is not straightforward to obtain reliable coefficients describing the frictional behavior between the intimal surface and the medical devices.

### *Finite element discretization*

One of the important aspects of the simulation of balloon angioplasty with stenting is the efficient discretization of the involved geometric models (artery, balloon, stent). Especially in those cases where multiple contact interactions occur, too fine meshes could lead to computationally expensive analysis.

As can be seen from Figure 1, the geometry of the investigated artery specimen is complex. Since the artery has a severe atherosclerotic narrowing the thickness and the curvature of the artery wall vary significantly along the axis of the artery. The finite element mesh was generated with the toolkit CUBIT<sup>34</sup> by using 4215 eight-node hexahedral elements. The generations of the meshes for the balloon and the stent required less amount of effort since their geometries do not present the same complexity. The design of the stent implied the use

of two-node 3D frame elements with six degrees of freedom for each node. For the stent the mesh was generated automatically through the algorithm mentioned above. The parameters that define the number of nodes for each strut are summarized in Figure 2b; a total of 525 nodes were used for the stent. The geometry of the balloon catheter is discretized by means of 195 eight-node hexahedral elements.

### *Loading procedure*

In order to simulate the physiological state of the artery, a displacement-controlled axial prestretch of 1.2 is applied at all nodes located on the end faces of the artery. At the end of this loading, the displacement boundary conditions are replaced by equivalent reaction forces. The mean artery pressure of 100 mmHg (13.3 kPa) is not taken into consideration in the simulation since the pressure loading is much smaller than the loads deriving from the contact interaction of the three bodies.

The expansion of the balloon-stent-artery system is simulated by using deformation dependent pressure loads, which are applied on the inner surface of the balloon. As the inner pressure increases, the balloon catheter comes into contact with the stent and after a further pressure increase both medical devices interact with the artery leading to the desired increase of the internal diameter of the artery wall. Finally, after full expansion of the balloon at an inner pressure of approximately 8 bar, the pressure loads are gradually removed, and only the stent remains in contact with the artery.

## **RESULTS AND DISCUSSION**

In this section the most important results of the performed computational analysis are presented. The outcome of “virtual” angioplasty with stenting by means of specific indicators is briefly presented. These indicators quantify the changes in the mechanical environment and the lumen area of the artery that occur during the dilation process.

One meaningful measure characterizing the success or failure of the treatment is the resulting change of the lumen area during and after angioplasty. We denote this measure as Lumen Gain, expressed through the factor  $LG$ <sup>12</sup>, and define as

$$LG = \frac{A_{l,cur}}{A_{l,ref}} - 1,$$

where  $A_{l,ref}$  is the area of the smallest cross-section of the inner artery wall before stenting, and  $A_{l,cur}$  is the related current area of the cross section at the same location.

Figure 4 shows the  $LG$  change at  $z = 17.5\text{mm}$  (location of the narrowest lumen area, compare with Figure 1), with respect to the internal balloon pressure  $p_b$  in bar. The inflation and deflation paths are illustrated by dashed lines with different intensity indicating stents with different strut diameters ( $stent_I$  and  $stent_{II}$ ).

As can be seen from Figure 4,  $stent_I$  with a strut thickness of 0.1 mm leads to  $LG = 0.81$  for full balloon inflation ( $p_b = 8$  bar), and to  $LG = 0.24$  when the balloon is removed. Likewise, when the simulation is performed with  $stent_{II}$ , having a strut thickness of 0.15 mm, the values  $LG = 0.67$  and 0.40 are obtained. These results indicate that at the end of the balloon inflation  $stent_I$  has a larger diameter, providing a higher  $LG$  value. However, as the balloon is gradually deflated and finally removed,  $stent_{II}$  with thicker struts leads to a significantly larger

lumen in comparison with stent<sub>I</sub>, indicating a more successful outcome of the treatment, as far as the lumen area is concerned.

As briefly implied above, the most significant drawback of angioplasty and stenting remains in-stent restenosis with lumen narrowing, mainly caused by vascular damage due to stent struts and non-physiological hemodynamics, and characterized by a fibroproliferative response and by increased matrix production. Elevated loads around the struts may lead to growth of the artery tissue and to a decreased success rate of the angioplasty treatment<sup>35</sup>. In addition, permanent, non-physiological strains, generated in the artery wall during and after stent expansion, may also lead to cellular proliferation<sup>9,36</sup> and finally to restenosis. All the above imply that stent optimization and the development of new stent designs is not a one parameter problem. Therefore, additional indicators, which allow the quantification of the changes in the mechanical environment of the artery, should be considered. An optimal treatment or stent design should, from a clinical point of view, lead to sufficiently enlarged lumen areas (large *LG* values), and at the same time it should not induce unnecessary artery trauma. The importance of each criterion for an optimization procedure depends on the specific patient and the related patient history.

Motivated by these thoughts, the generated contact pressure, i.e. the pressure between the stent struts and the surface of the intima, is further analyzed. Figure 5 illustrates the contact pressure  $p_c$  on the inner surface of the artery wall for both cases (stent<sub>I</sub> and stent<sub>II</sub>) after complete deflation and removal of the balloon catheter ( $p_b = 0$  bar). A comparison of the obtained computational results between the two stent configurations indicates that, as expected, for the case of the stiffer stent<sub>II</sub> the generated contact pressure is approximately two times higher compared to stent<sub>I</sub>, while the pressure field retains almost the same pattern.

Interestingly, the position of the highest pressure is located around the horizontally positioned struts of the stents.

The purpose of the work by Holzapfel et al.<sup>11</sup> was also concerned with the determination of the mechanical environment present after angioplasty. Therein, an anisotropic material model was used to describe the mechanical response of the artery wall, while, as in most studies documented in the literature, the balloon catheter was not considered. However, a stent was considered to be in contact with the artery wall during the expansion phase. Results that are of particular interest are depicted in Figure 6, showing distributions of circumferential and axial (Cauchy) stresses on the inner and outer artery surfaces after stent deployment and at an intraluminal pressure of 13.3 kPa. In the figure the stent itself is not shown for illustrative purposes. In order to visualize the inner artery wall, the plaque region has been partly left out. The location of the stent is indicated by dashed lines.

Local stress concentrations near the stent edges can clearly be appreciated. They are mainly due to the compliance mismatch in the mechanical properties between the stented and the immediately adjacent regions. At the stent edges an increased presence of neointimal hyperplasia is documented which may at least in part result from the occurring non-physiological hemodynamics at those locations (disturbed flow, decreased distal perfusion, etc.).

Interestingly, while the circumferential stresses at these sites are tensile, as expected, see Figure 6(a), the axial stresses are compressive, see Figure 6(b). Even more remarkable is the fact that the adventitia exhibits high axial tensile stresses at the corresponding locations (not shown). Figure 6 illustrates the complex three-dimensional and layer-specific stress-strain states caused by the stent-artery interaction. It is obvious that the 3D stress-strain state depends strongly on the lesion-morphology and the utilized stent type.

In addition, the study of Holzapfel et al.<sup>11</sup> indicated that the stresses are higher in the non-diseased artery wall than in the plaque region since the thickness of the non-diseased wall is smaller. Recently, this result was confirmed by Gasser and Holzapfel<sup>37</sup>, a study in which a model was proposed to trace fissuring and/or dissection in atherosclerotic plaques during balloon angioplasty interventions. The predicted results therein indicate that plaque fissuring and dissection cause localized mechanical trauma, but prevent the main portion of the stenosis from high stress, and hence from continuous tissue damage.

## **SUMMARY AND CONCLUSION**

In this communication one particular approach has been reviewed to provide a better understanding of stented artery solid mechanics and related formation of neointimal hyperplasia and restenosis. Because of the inherent small stent struts and the overall geometric, structural and material complexities of the underlying problem, computational methods and graphics capability to display three-dimensional results are particularly useful for predicting short and long-time mechanobiological phenomena, and, therefore, to improve diagnostics, treatment planning and current stent designs. Herein we have focused on the biomechanics of the artery wall which is severely affected by the overall stent design, in particular the mesh geometry of the stent struts.

On the basis of a human femoral artery with severe atherosclerotic narrowing, for which a complete set of geometric and mechanical data was available, we have outlined a methodology to predict the 3D mechanical changes in the artery wall which occur during angioplasty with stent deployment. The geometric model was re-constructed from high-resolution MR images, while the mechanical response of the artery wall, which was assumed

to be homogeneous, was described by an isotropic, hyperelastic model able to capture the nonlinear effects of artery tissues at the finite strain domain. The material parameters were obtained from uniaxial extension tests on stripes extracted from femoral arteries. The outlined model approach considered also the axial *in situ* pre-stretch of the artery. Besides the homogeneity and isotropy assumptions, the artery model did not address damage mechanisms, which occur due to vascular injury during the stent deployment. In addition, residual artery stresses were neglected.

Based on a balloon-expandable stent product which was previously commercially available the geometric structure was parameterized to allow convenient changes. Two stent designs were considered with basically the same geometric model but with different strut thickness providing the basis for a comparison of their performances. Both stents were analyzed by making use of an elastoplastic model. Finally, the mechanical response of the balloon catheter was described by a cylindrically orthotropic model, assuming that the balloon responds (almost) non-compliant in the axial direction and allows a very soft response in the circumferential direction at low internal pressure and exposing a stiffening effect at higher pressure values. The loading procedure involved the inflation of the balloon catheter up to approximately 8 bar, leading to a stent expansion, and then the complete deflation of the balloon was considered.

In order to obtain a better judgment of the performance of the two considered stents, a meaningful scalar indicator was introduced, namely the one characterizing the lumen gain, which should be as large as possible. In addition, it is also informative to analyze the contact pressure between the stent struts and the surface of the intima, which should be as small as possible.

The patient-specific analysis has identified larger lumen gain for the case of stent<sub>II</sub> with thicker stent struts, but also higher contact pressures and higher circumferential and axial strains when compared with the values obtained from stent<sub>I</sub> with thinner struts. This finding suggests that even though stent<sub>II</sub> leads to a larger lumen, it is not necessarily the optimal solution since severe mechanical changes (stresses, strains) in the artery wall might be responsible for the development of cell proliferation and restenosis. Because of the many factors that influence restenosis formation it is difficult to interpret how much such mechanical changes in the artery wall affects clinically observed restenosis.

The documented methodology serves as a biomechanical basis to predict the effects a deployed stent has on the artery wall, and may serve to improve current stent designs on a lesion-specific basis.

## **REFERENCES**

1. Serruys PW, de Jaegere P, Kiemeneij F, et al. A comparison of balloon-expandable-stent implantation with balloon angioplasty in patients with coronary artery disease. Benestent Study Group. *N Engl J Med* 1994; 331:489–495.
2. Hoher M, Wohrle J, Grebe OC, et al. A randomized trial of elective stenting after balloon recanalization of chronic total occlusions. *J Am Coll Cardiol* 1999; 34:722–729.
3. Thom T, Haase N, Rosamond W, et al. Heart disease and stroke statistics – 2006 update. A report from the American Heart Association Statistics Committee and Stroke Statistics Subcommittee. *Circulation* 2006; 113:e85–e151.

4. Burton HM, Hunter WL. Drug-eluting stents: A multidisciplinary success story. *Adv Drug Deliv Rev* 2006; 58:350–357.
5. Fattori R, Piva T. Drug-eluting stents in vascular intervention. *Lancet* 2003; 361:247-249.
6. Kastrati A, Mehilli J, Dirschinger J, et al. Intracoronary stenting and angiographic results: strut thickness effect on restenosis outcome (ISAR-STEREO) trial. *Circulation* 2001; 103:2816–2821.
7. Pache J, Kastrati A, Mehilli J, et al. Intracoronary stenting and angiographic results: strut thickness effect on restenosis outcome (ISAR-STEREO-2) trial. *J Am Coll Cardiol* 2003; 41:1283–1288.
8. Edelman ER, Rogers CR. Pathobiologic responses to stenting. *Am J Cardiol* 1998; 81:4E-6E.
9. Wang DL, Wung BS, Shyy YJ, et al. Mechanical strain induces monocyte chemotactic protein-1 gene expression in endothelial cells. Effects of mechanical strain on monocyte adhesion to endothelial cells. *Circ Res* 1995; 77:294–302.
10. Schwartz RS, Henry TD. Pathophysiology of coronary artery restenosis. *Rev Cardiovas Med* 2002; 3, Suppl. 5:S4–S9.
11. Holzapfel GA, Stadler M, Schulze-Bauer CAJ. A layer-specific three-dimensional model for the simulation of balloon angioplasty using magnetic resonance imaging and mechanical testing. *Ann Biomed Eng* 2002; 30:753–767.
12. Holzapfel GA, Stadler M, Gasser TC. Changes in the mechanical environment of stenotic arteries during interaction with stents: Computational assessment of parametric stent design. *J Biomech Eng* 2005; 127:166–180.

13. Lally C, Dolan F, Prendergast PJ. Cardiovascular stent design and vessel stresses: a finite element analysis. *J Biomech* 2005; 38:1574–1581.
14. Bedoya J, Meyer CA, Timmins LH, Moreno MR, Moore JE. Effects of stent design parameters on normal artery wall mechanics. *J Biomech Eng* 2006; 128:757–765.
15. Liang DK, Yang DZ, Qi M, Wang WQ. Finite element analysis of the implementation of a balloon expandable stent in a stenosed artery. *Int J Cardiol* 2005; 104:314–318.
16. Migliavacca F, Petrini L, Massarotti P, Schievano S, Auricchio F, Dubini G. Stainless and shape memory alloy coronary stents: a computational study on the interaction with the vascular wall. *Biomech Model Mechanobio* 2004; 2:205–217.
17. Kioussis DE, Gasser TC, Holzapfel GA. Smooth contact strategies with emphasis on the modeling of balloon angioplasty with stenting. *Int J Numer Meth Eng*, in press.
18. Moreno MR, Bedoya J, Meyer C, Moore Jr., JE. Computational modeling of stented arteries: considerations for evolving stent designs. In: “Mechanics of Biological Tissue”, GA Holzapfel, RW Ogden (eds.), Springer-Verlag, Heidelberg, 2005.
19. Duraiswamy N, Schoephoerster RT, Moreno MR, Moore, Jr., JE. Stented artery flow patterns and their effects on the artery wall. *Annu Rev Fluid Mech* 2007; 39:357–82.
20. Stary HC. *An Atlas of Atherosclerosis Progression and Regression*. Parthenon, New York, 1999.
21. Auer M, Stollberger R, Regitnig P, Ebner F, Holzapfel GA. 3-D reconstruction of tissue components for atherosclerotic human arteries based on high-resolution MRI. *IEEE T Med Imaging* 2006; 25:345–357.
22. Rhodin JAG. Architecture of the vessel wall. In: “Handbook of Physiology, The Cardiovascular System”, DF Bohr, AD Somlyo, HV Sparks (eds.), Volume 2, pp. 1–31, American Physiological Society, Bethesda, Maryland, 1980.

23. Cox RH, Detweiler DK. Arterial wall properties and dietary atherosclerosis in the racing greyhound. *Am J Physiol* 1979; 236:H790–H797.
24. Holzapfel GA, Schulze-Bauer CAJ, Stadler M. Mechanics of angioplasty: wall balloon and stent. In: “Mechanics in Biology”, J Casey, G Bao (eds.), pp.141–156, The American Society of Mechanical Engineers (ASME), New York, AMD-Vol. 242/BED-Vol. 46, 2000.
25. Holzapfel GA, Sommer G., Regitnig P. Anisotropic mechanical properties of tissue components in human atherosclerotic plaques. *J Biomech Eng* 2004; 126:657–665.
26. Holzapfel GA, Sommer G., Gasser CT, Regitnig P. Determination of layer specific mechanical properties of human coronary arteries with non-atherosclerotic intimal thickening, and related constitutive modelling. *Am J Physiol Heart Circ Physiol* 2005; 289:H2048–2058.
27. Holzapfel GA. Determination of material models for arterial walls from uniaxial extension tests and histological structure. *J Theor Biol* 2006; 238: 290–302.
28. Holzapfel GA, Sommer G, Auer M, Regitnig P, Ogden RW. Layer-specific 3D residual deformations of human aortas with non-atherosclerotic intimal thickening. *Ann Biomed Eng*, in press, DOI 10.1007/s10439-006-9252-z.
29. Cox RH. Passive mechanics and connective tissue composition of canine arteries. *Am J Physiol* 1978; 234:H533–H541.
30. Delfino A, Stergiopoulos N, Moore Jr. JE, Meister JJ. Residual strain effects on the stress field in a thick wall finite element model of the human carotid bifurcation. *J Biomech* 1997; 30:777–786.
31. Schulze-Bauer CAJ, Mörth CM, Holzapfel GA. Passive biaxial mechanical response of aged human iliac arteries. *J Biomech Eng* 2003; 125:395–406.

32. Kiouisis DE, Gasser TC, Holzapfel GA. A numerical model to study the interaction of vascular stents with human atherosclerotic lesions. *Ann Biomed Eng*, in press.
33. Grüntzig A, Kumpe DA. Technique of percutaneous transluminal angioplasty with Grüntzig balloon catheter. *Am J Radiol* 1979; 132:547–552.
34. CUBIT Team. CUBIT 10.0 User's Manual. Sandia National Laboratories, Albuquerque, New Mexico, USA, 2005.
35. König A, Schiele TM, Rieber J, Theisen K, Mudra H, Klauss V. Influence of stent design and deployment technique on neointima formation and vascular remodeling. *Z Kardiol* 2002; 91:98–102.
36. Leung DY, Glagov S, Mathews MB. Cyclic stretching stimulates synthesis of matrix components by arterial smooth muscle cells in vitro. *Science* 1976; 191:475–477.
37. Gasser TC, Holzapfel GA. Modeling plaque fissuring and dissection during balloon angioplasty intervention. *Ann Biomed Eng*, in press.

## FIGURES

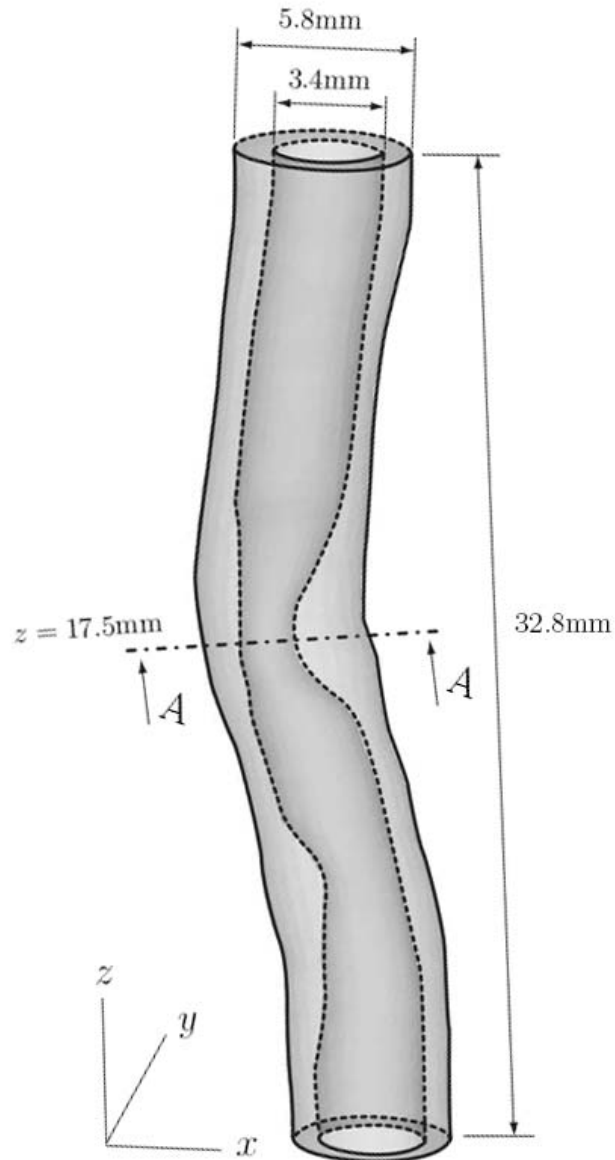
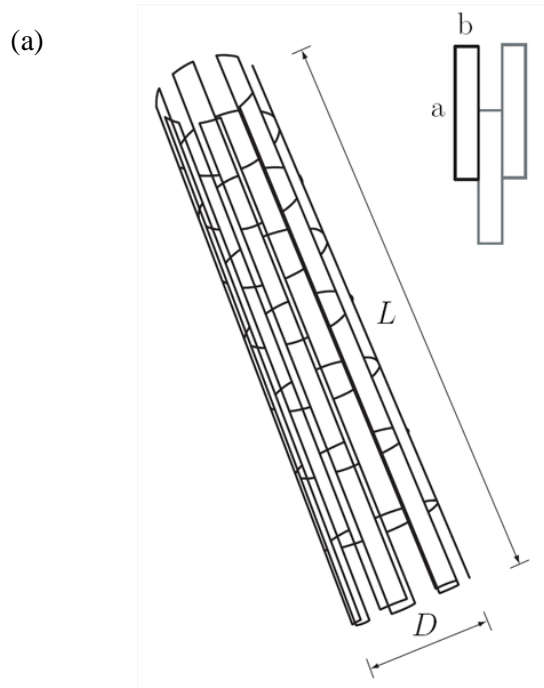


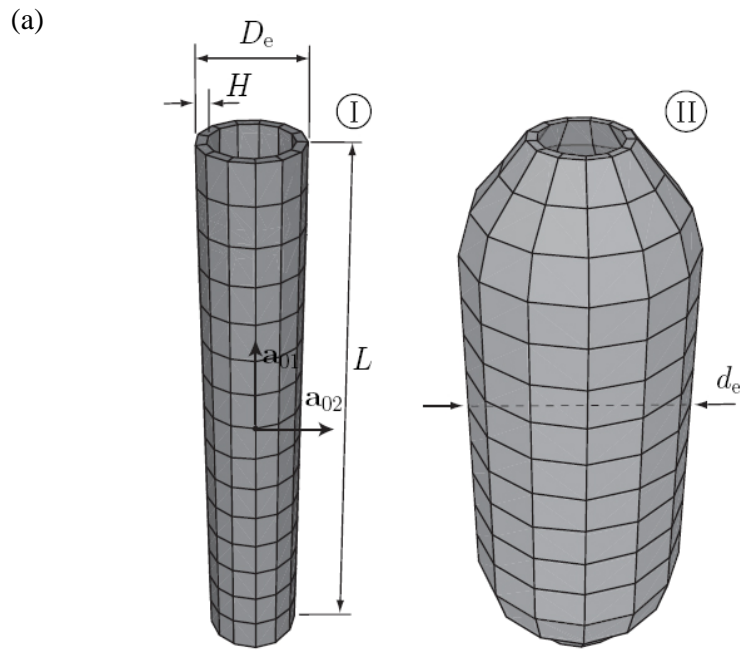
Figure 1: Patient-specific, three-dimensional geometric model of an atherosclerotic femoral artery with a lesion of type  $V^{20}$  constructed on the basis of high-resolution MR images and NURBS.



(b)

<b>Stent design and discretization parameters</b>	
Length $L$	10 mm
Diameter $D$	2 mm
Number of axial cells	4
Number of circumferential cells	7
Strut thickness	0.1, 0.15 mm
Nodes on strut a	24
Nodes on strut b	3

Figure 2: Geometric model of a Palmaz-Schatz™ balloon-expandable stent: (a) undeformed configuration; (b) stent design and discretization parameters used for the automatic generation of the geometry and the finite element mesh.



(b)

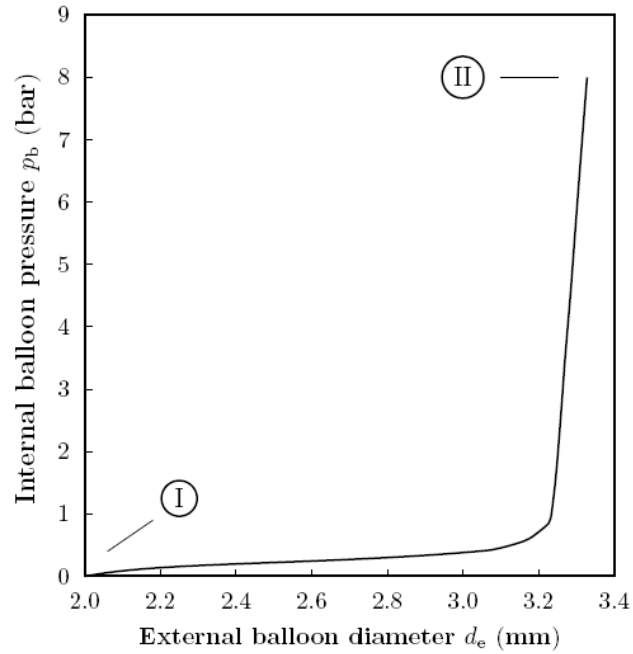


Figure 3: Finite element simulation of the dilation of a Grüntzig-type balloon catheter: (a) finite element mesh in the undeformed (I) and the deformed (II) configuration at 8 bar of internal pressure; (b) relation between the internal balloon pressure and the external balloon diameter.

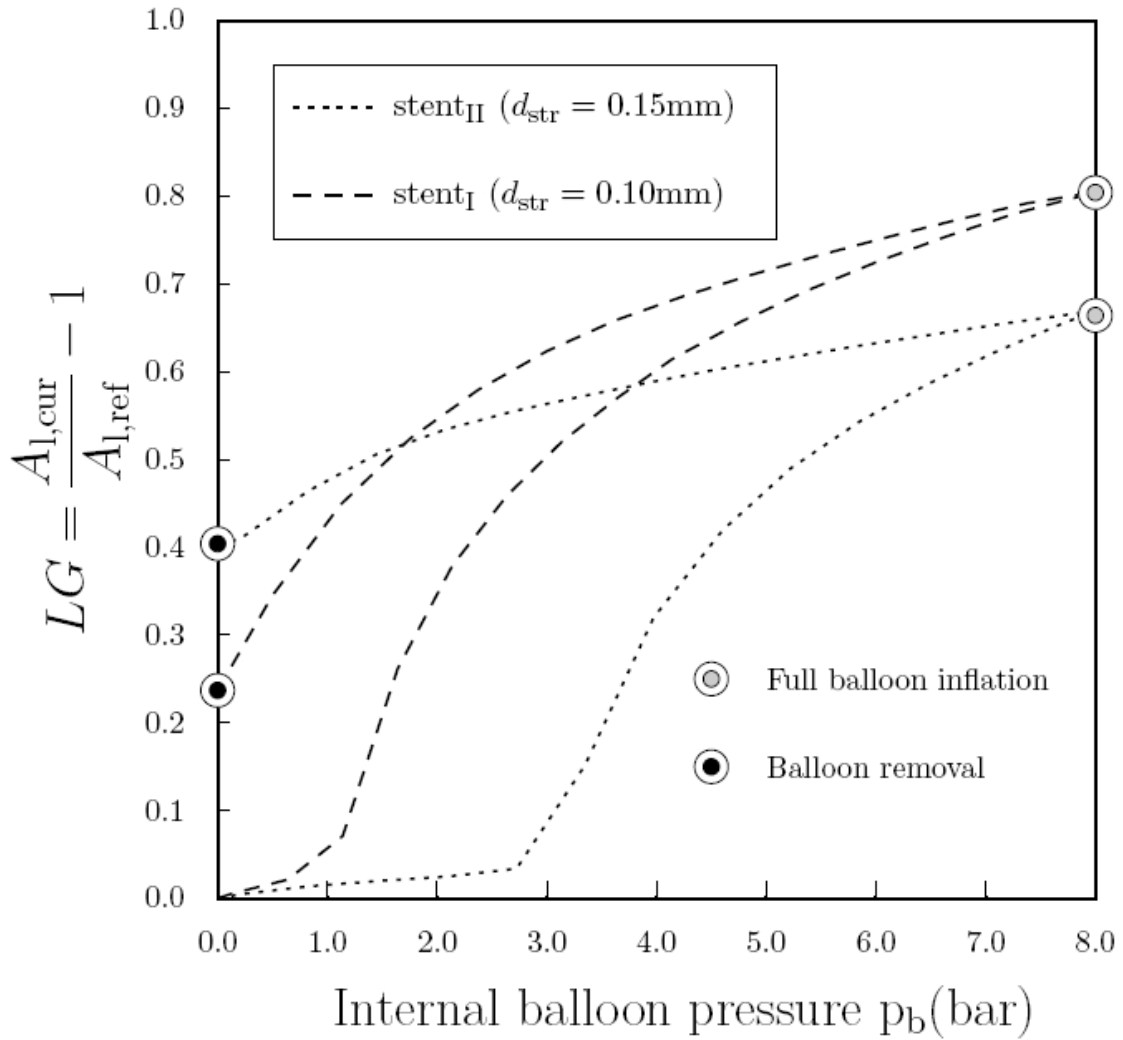


Figure 4: Lumen gain  $LG$  versus internal balloon pressure  $p_b$  at the narrowest lumen area of the arterial wall, i.e. at  $z = 17.5\text{mm}$  (compare with Figure 1). The two curves indicate the change of  $LG$  along the inflation and deflation paths of the balloon for two stent designs with different strut diameters indicated as  $\text{stent}_I$  and  $\text{stent}_{II}$ .

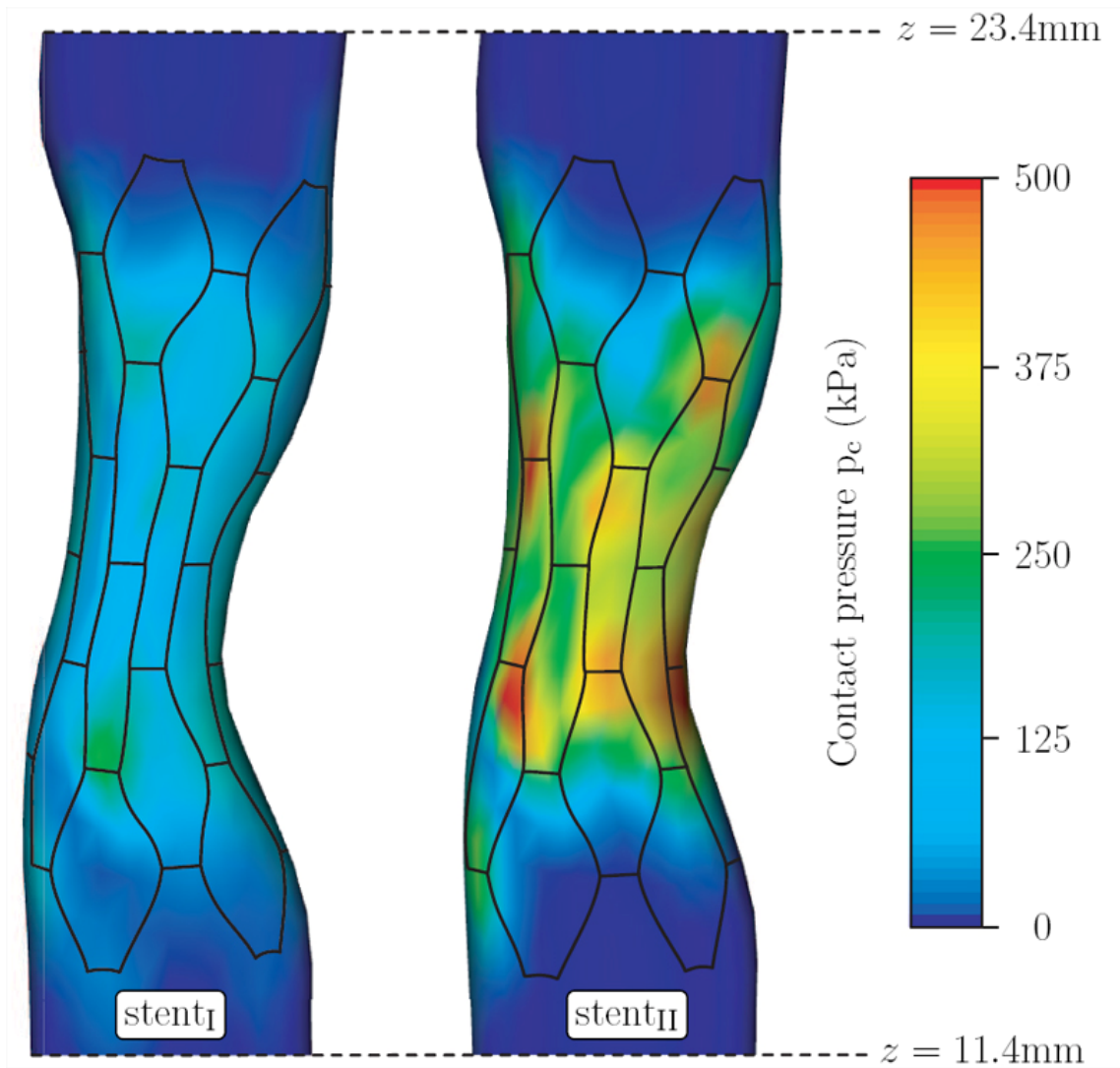


Figure 5: Distribution of the contact pressure  $p_c$ , i.e. the pressure between the stent struts and the surface of the inner artery wall, after complete deflation and removal of the balloon catheter. Pressure distributions are shown for stent<sub>I</sub> (with strut thickness 0.1 mm) and for stent<sub>II</sub> (with strut thickness 0.15 mm).

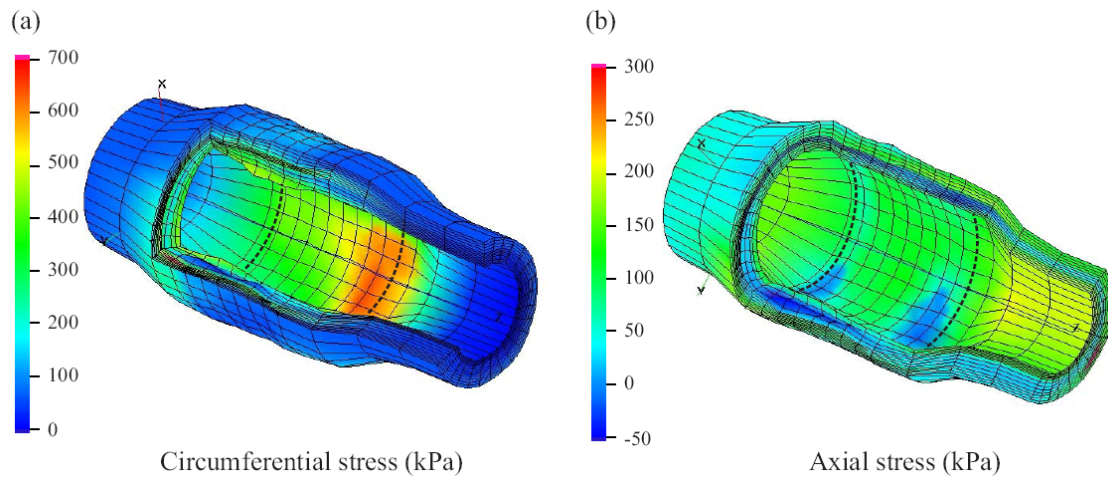


Figure 6: Circumferential (a) and axial stress distributions (b) for a human stenotic artery at an intraluminal pressure of 13.3 kPa after stent deployment. At the stent edges, indicated by dashed lines, local stress concentrations occur.